## **NJC**



### **PAPER**



Cite this: New J. Chem., 2024, 48.1607

Received 7th May 2023, Accepted 18th December 2023

DOI: 10.1039/d3nj02100a

rsc.li/njc

# Chemical fuel energy driving polymerization towards porous carbon nitride for energy storage application†

Tatyana Jackson, Schindra Kumar Ray, Kiran Subedi, Tansir Ahamad oc Bishnu Prasad Bastakoti \*\*

A chemical reaction network has been utilized as an energy and radical source to drive a polymerization of acrylonitrile monomer in an aqueous solution. The polymer is formed in a polymerization-induced self-assembly fashion. The carbonization of polyacrylonitrile leads to the formation of nanoporous carbon nitride. Ru species are observed in the porous polymer and carbon nitride. Tris (2,2'-bipyridyl) ruthenium(II) chloride hexahydrate, a catalyst used in the B-Z reaction, remains in the carbon nitride framework, enhancing the electronic and chemical properties of the composites. The electrochemical properties of the composites were studied using cyclic voltammetry, galvanostatic charge-discharge, and electrochemical impedance spectroscopy. The specific capacitance of the electrode was found to be 763 F  $g^{-1}$  at 0.3 A  $g^{-1}$  current densities. The excellent specific capacitance behavior is mainly attributed to micro/mesopores structure, active sites for a superior redox reaction, intimate contact between Ru/RuO2 nanoparticles with amorphous carbon nitride, rapid transportation of ions, and fast electrolyte transfer process.

#### Introduction

Carbon-based nanomaterials are widely employed for their beneficial attributes, such as their lightweight size, reduced thermal expansion, increased conductivity, biocompatibility, and exceptional stiffness. These features drive the interest for those materials in development, innovation connected with energy transformation, metal-free catalysts, bio applications, aviation, and automotive industries. 1,2 Among the different forms of advanced carbon materials, porous carbon has attracted the interest of scientific communities due to its high surface area, pore volumes, and easy diffusion of ions/molecules. 3-9 Equipping carbon with different-sized pores and shapes lowers the density of the materials and expands its surface area to accelerate interfacial energy and mass transfer, which is crucial and decisive in many surface-related physical and chemical processes. The addition of heteroatoms influences electronic, structural, and surface-active properties. 10-13

The choice of polymer to synthesize the heteroatom-doped porous carbon materials is of tremendous significance due to the availability of various macromolecular and self-assembled (nano)structures, tunable chemical compositions, and versatile processing techniques.<sup>14</sup> One of the most fundamental characteristics of polymers is their ability to form versatile morphologies via phase separation in selective solvents. 15 Various beautiful mesostructures, such as cubes, cylinders, or lamellae, can be well constructed, especially with different chemical compositions. N-doped mesoporous carbon spheres were synthesized through self-polymerization of dopamine and spontaneous assembly of poly(styrene-b-ethylene oxide) micelles. The N-doped carbon spheres were obtained with a remarkably uniform mesopore size of 16 nm. Similarly, Zhao et al. utilized the micelle fusion-aggregation assembly method and successfully constructed N-doped mesoporous carbon materials. 16 N-doped bicontinuous gyroid mesoporous carbon was synthesized using poly(ethylene oxide-b-caprolactone) block copolymer as a soft template with melamine. The dopant's homogeneity is missing when a secondary source for the dopant is used.<sup>17</sup>

Directly carbonizing nitrogen and carbon-containing compounds without an external template and a dopant source reduces the template-related etching/extraction procedure. It overcomes the non-uniform distribution of dopants in the carbon framework. By adjusting the structure of the polymer and pyrolysis program, the content of heteroatom and porosity

<sup>&</sup>lt;sup>a</sup> Department of Chemistry, North Carolina A&T State University, 1601 E Market Street Greensboro., NC 27411, USA. E-mail: bpbastakoti@ncat.edu

<sup>&</sup>lt;sup>b</sup> Analytical Services Laboratory, North Carolina A&T State University, 1601 E Market Street Greensboro, NC 27411, USA

<sup>&</sup>lt;sup>c</sup> Department of Chemistry, King Saud University Riyadh, Saudi Arabia

<sup>†</sup> Electronic supplementary information (ESI) available: Oscillation profile, NMR, and TEM images. See DOI: https://doi.org/10.1039/d3nj02100a

can be controlled. Urea, melamine, thiourea, and dicyandiamide were carbonized under the same thermal conditions and found different physicochemical properties of carbon nitride. The formation of gases such as CO2, H2S, NH3, and water vapor during pyrolysis favors the expansion of the packing layers and porous structure. 18 Burmeister et al. synthesized graphitic carbon nitride via polycondensation of dicyandiamide in the presence of eutectic salt melt. The size of anions plays a vital role in templating effects. 19 Mesoporous carbon nitride was synthesized by casting molecular precursors on mesoporous silica. The silica matrix was kept in cyanamide solution at a temperature greater than its melting point and calcined at 550 °C in N<sub>2</sub>, followed by removing silica by hydrogen fluoride.<sup>20</sup>

Here, we used redox chemistry as an energy source to initiate polymerization in a polymerization-induced self-assembly way to synthesize polymer in an aqueous solution. Carbon and nitrogen-containing monomers (acrylonitrile) were taken as the building units for carbon nitrides upon calcination in an inert medium. TEM measurements revealed that Ru/RuO<sub>2</sub> nanoparticles were anchored on the carbon nitride framework. Those nanoparticles were derived from the catalyst used in the B-Z reaction. It is a straightforward method to synthesize porous carbon nitride composites. The porous carbon nitride formation process was proposed, and the morphology, structural, and chemical characteristics have been systematically studied. The one-pot synthesis allows it to get porous polymer with catalyst retention. The study of electrochemical properties exhibits that porous carbon nitride has potential applications in energy storage application.

#### Materials and method

Sulfuric acid (H<sub>2</sub>SO<sub>4</sub>; Alfa Aesar), malonic acid (Alfa Aesar), sodium bromate (Thermo Scientific) tris (2,2'-bipyridyl) ruthenium(II) chloride hexahydrate (Tokyo Chemical Industry; Ru(bpy)<sub>3</sub>Cl<sub>2</sub>·6H<sub>2</sub>O) acrylonitrile (Sigma Aldrich), potassium hydroxide (KOH; Thermo Scientific), Nafion (Sigma Aldrich) were used without further purification. Stock solutions were prepared in deionized water.

The following chemicals were added sequentially for the synthesis of polyacrylonitrile: 309.32 mL distilled water, 20 mL (0.6 M) malonic acid, 40 mL (1 M) sodium bromate, 24 mL (5 M)  $H_2SO_4$ , 2 mL acrylonitrile monomer and 4.68 mL (8.5  $\times$  10<sup>-3</sup> M) Ru(bpy)<sub>3</sub>Cl<sub>2</sub>·6H<sub>2</sub>O. The solution was stirred at room temperature for 3 hours. The reaction vessels were covered with aluminum foil to reduce the interference from visible light. The polymer was collected via centrifuge, dried, and calcined at 600 °C at a ramping rate of 5 °C min<sup>-1</sup> in nitrogen.

#### Characterization

The change in potential during the B-Z reaction was monitored using the SPER benchtop redox electrode. The polymer's molecular structure was characterized with a Bruker Ascend<sup>TM</sup> 400 MHz proton NMR spectrometer. The crystallographic study of the sample was carried out by powder X-ray diffractometer technique using Rigaku Mini Flex 600. Elemental analysis of the samples was conducted using the PerkinElmer CHN Analyzer 2400 series II. JEOL JSM-IT800 Schottky FESEM and JEOL TEM 1210 electron microscope were used to observe the external surface and internal structure, respectively. An X-ray photoelectron spectroscopy (Thermofisher Scientific, Waltham, MA, USA), from Physical Electronics 5600ci with ultra-high vacuum ( $\sim 6 \times 10^{-9}$  Torr), Al K $\alpha$ source, analyzer diameter of 200 nm, and PHI Multipack 9.4, was used to study the chemical composition of the nanoparticles. The Fourier transform infrared data was collected from the IRTracer-100 Shimadzu instrument in ATR mode. A Quantachrom surface area analyzer obtained N<sub>2</sub> adsorption-desorption isotherms.

To prepare the sample electrodes, a piece of nickel foam was washed with 2 M HCl, water, and ethanol to remove the impurities. Then, the slurry was prepared by using 4 mg of sample in 0.5 mL ethanol and 50 µL of Nafion. The slurry was deposited on the surface of nickel foam  $(1 \times 1 \text{ cm}^2)$ . It was dried in an oven at 70 °C for 10 h. An aqueous KOH (3 M) solution was used as an electrolyte in electrochemical measurements. Ni foam, Ag/AgCl, and Pt wire represent the working, reference, and counter electrodes, respectively. The electrochemical measurements were obtained using the CH instrument. The cyclic voltammetry (CV) was measured from 20 to 80 mV s<sup>-1</sup> at scanning rates of -0.3 to 0.7 V. Galvanostatic charge-discharge (GCD) analysis was also performed (current density: 0.3 to 1 A g<sup>-1</sup> and voltage: 0.1 to 0.4 V). In addition, electrochemical impedance spectroscopy (EIS) was investigated from 0.01 Hz to 100 kHz. Furthermore, the specific capacitance of the electrode material was calculated from GCD curves using the following equation;

$$C_{\rm s} = \frac{I \cdot \Delta t}{m \cdot \Delta V}$$

where  $C_s$ , I,  $\Delta t$ , m, and  $\Delta V$  indicate the specific capacitance  $(F g^{-1})$ , charge/discharge current (A), discharge time (s), the mass of the material (g), and potential window (V), respectively.

#### Results and discussion

The B-Z reaction is the most studied oscillatory chemical reaction. It comprises the oxidation of the malonic acid by the bromate anion in the presence of a strong acid catalyzed by transition metal ions. Zaikin and Zhabotinsky studied the detailed mechanism of the reaction.21 It has potential applications in materials synthesis, sensing, and chemical computing.22,23 Among the radicals produced, malonyl (MA\*), bromous (BrO2\*), and Ru(bpy)\* radicals are the three prominent radicals that initiate polymerization during the oscillation of the B-Z reaction.<sup>24-26</sup> Tris (2,2'-bipyridyl)ruthenium(II) chloride hexahydrate and acrylonitrile (nitrogen and carbon-containing monomer) were used as catalyst and monomer respectively, to synthesize the polymer aqueous solution. The progress of B-Z reaction was monitored by measuring the electrode potential values of reduced and oxidized species of Ru catalyst. The catalyst complex's central metal atom (Ru) undergoes periodic redox reactions. Ru<sup>2+</sup> and Ru<sup>3+</sup> ions possess different potential values (Fig. S1, ESI†). Ru(bpy)<sub>3</sub>Cl<sub>2</sub> catalyst alone can be used as a

photocatalyst for the polymerization reaction in visible light.<sup>27</sup> It has strong absorption on the visible range and could efficiently promote free radical polymerization. To avoid the contribution of Ru(bpy)\* in the polymerization reaction, the polymerization reaction was carried out in the dark. Other transition metal salt/ complexes such as Ce4+, Mn2+, and Feroin could be used as catalysts. 28 The B-Z recipe and monomer are mixed and stirred constantly. The induction time was delayed, and the B-Z reaction propagated with a lower amplitude in polymerization (Fig. 2). The oscillation of the B-Z response is somewhat perturbed during polymerization. However, B-Z oscillations go on for several hours. The extension of the molecular chain of acrylonitrile occurs by seizing some intermediates. Sciascia et al. studied the effects of macromolecules on the oscillation of the B-Z reaction in solution. The numerical simulation with MBM modeling and physicochemical study show that molecules' viscosity and diffusion strongly influence the B-Z reaction's nonlinear behavior.<sup>29</sup> The clear solution turns turbid, indicating the formation of polyacrylonitrile. Acrylonitrile is water-soluble in the monomer and insoluble when it gets polymerized. The visual appearance of polymer formation from a clear monomer solution in an aqueous solution was observed (Fig. 2 inset). Fig. S2 (ESI†) shows the <sup>1</sup>H-NMR spectra of polyacrylonitrile. The 2.24 ppm and 3.13 ppm peaks correspond to the C-H backbone of polyacrylonitrile. The formation of polyacrylonitrile was also confirmed by XRD and FTIR measurements. The unique diffraction peak that appeared at  $2\theta$  at  $17.4^{\circ}$  (Fig. S3a, ESI†) ensures the formation of polyacrylonitrile. The polymer was directly carbonized without further purification. After calcining the asprepared sample at 600 °C in N<sub>2</sub> condition, the original peaks of the pure polymer disappeared, and a broad hump at 25° confirmed the amorphous carbon nitride. The residue oxygen

in the system initiates the cyclization of polyacrylonitrile during carbonization.<sup>30</sup> The XRD peaks at 37.7 (101) and 43.9 (200) are identified as RuO2 crystals;31 and 77.4 (103) and 81.5 (112) are for Ru crystals.32 Ru and RuO2 formed during the oxidationreduction cycle of the B-Z reaction and carbonization. Despite its ruthenium content, the primary carbon nitride material lacks crystalline peaks. Amorphous carbon nitride with crystalline Ru/ RuO<sub>2</sub> makes up the composite material. Fig. 3a depicts the FTIR spectra of monomer, polymer, and carbon nitride. The peaks at 2231 cm<sup>-1</sup> and 685 cm<sup>-1</sup> are identified for the nitrile (CN) and vinyl (CH<sub>2</sub>=CH) of monomers, respectively. The stretching and bending vibration of methylene (-CH<sub>2</sub>) is observed at 965 cm<sup>-1</sup> and 1411 cm<sup>-1</sup>, respectively. The polyacrylonitrile FTIR spectrum shows nitrile's characteristic stretching vibrational peak (-CN) at 2242 cm<sup>-1</sup>, and CH<sub>2</sub> at 2900 cm<sup>-1</sup>. The additional peaks on the polymer are due to other chemicals used in the synthesis.

Microscopy images of as-prepared polyacrylonitrile show the surface morphology and internal structure (Fig. S4, ESI†). It is interesting to observe the porosity of the polymer. In general, soft templates or hard templates are used to create porosity. In our synthesis, several gases (such as CO2 and Br2) are produced during the oscillation of the B-Z reaction, which acts as a template to generate pores. 34,35 Fig. 1c shows the TEM images of calcined samples showing the porous structure of CN. The high-resolution TEM images showed Ru/RuO2 nanoparticles firmly anchored on the surface of carbon nitride. Ru and RuO2 were derived from the catalyst used for the B-Z oscillation.

The Raman peaks at 1347 cm<sup>-1</sup> and 1584 cm<sup>-1</sup> correspond to the D and G bands, respectively. G band results from in-plane vibration of sp<sup>2</sup> bonded C atoms with  $E_{2g}$  symmetry. The D band is a breathing mode with A<sub>1g</sub> symmetry due to

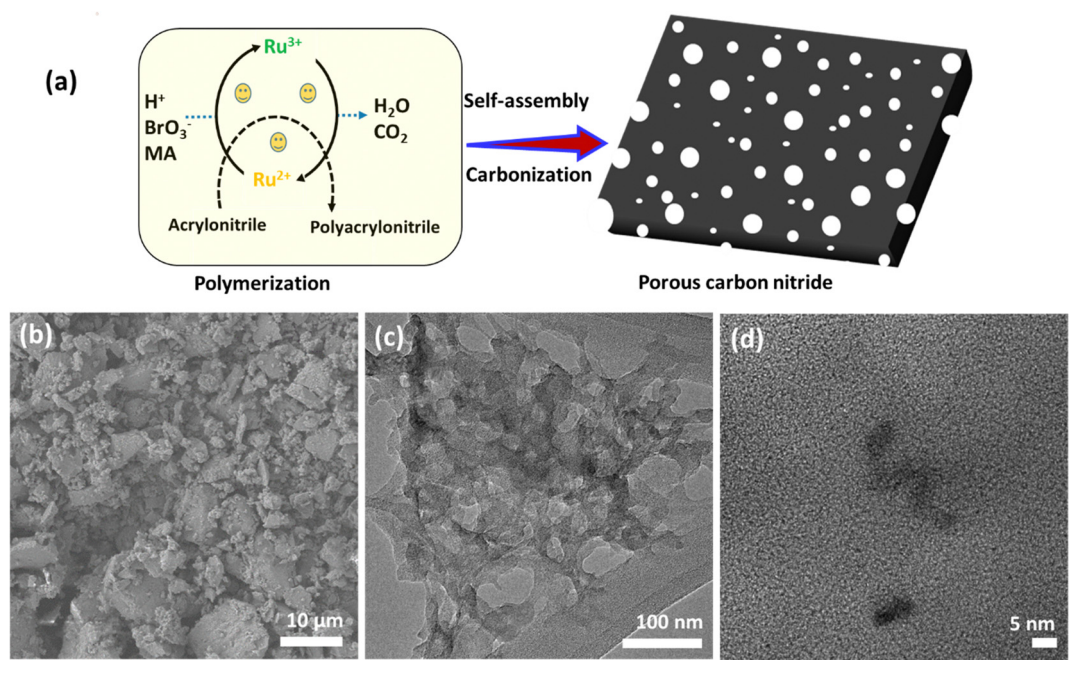


Fig. 1 (a) Schematic illustration of formation of porous carbon nitride. (b)-(d) Electron microscopy images of porous carbon nitride composites.

Paper NJC

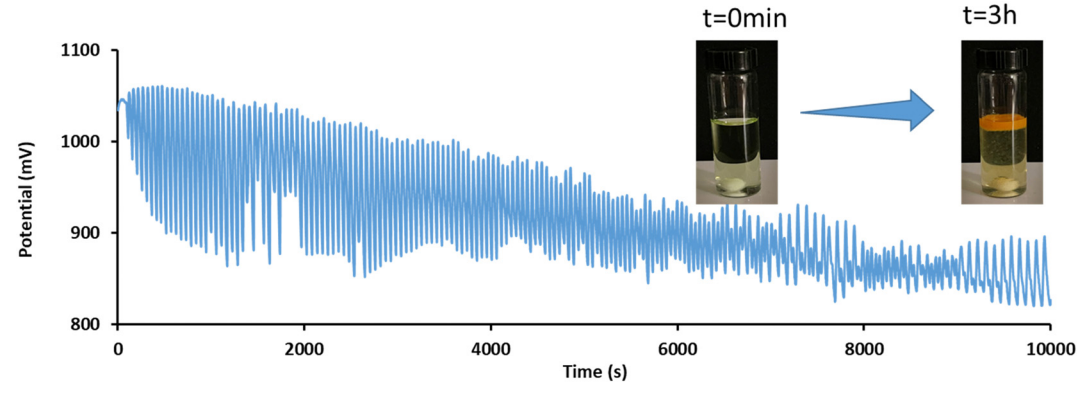


Fig. 2 The periodic change in potential of B–Z reaction during polymerization. The inset image shows the reaction solution before and after polymerization for 3 h.

structural defects. <sup>36</sup> The higher value of D over G signifies a disordered structure. 1.26  $I_{\rm D}/I_{\rm G}$  ratio value indicates the amorphous nature of the carbon nitride. The CHN analysis was performed, and 63.4% carbon, 17.83% nitrogen, and 2.29% hydrogen were observed. The uniform distribution of carbon and nitrogen was also confirmed in SEM EDX (Fig. S5, ESI†). In addition, the nitrogen adsorption–desorption isotherms were recorded (Fig. 3b). The BET surface area was found to be 44 m<sup>2</sup> g<sup>-1</sup> with an average pore diameter of 4.5 nm. The pore diameter was calculated by the BJH method.

XPS determined the elemental makeup of the carbon nitride surface and was also used to determine the chemical state of the catalytic Ru species. The XPS survey spectrum is shown in Fig. 4, with four prominent peaks corresponding to O1s, N1s, and C1s with an overlapping Ru 3d peak at roughly 532, 399, and 284 eV, respectively. Two binding environments were discovered with binding energies of 285 and 283 eV, attributed to ruthenium oxide and ruthenium metal, respectively (Fig. 4a).<sup>37</sup> This confirms with XRD analysis that the catalyst formed into a metal oxide throughout the calcination process. The C1s (Fig. 4b) show three distinctive peaks at 284, 285, 283 eV, which are ascribed to C=C, C-N/C-O, and a tiny peak from the interaction between

carbon and ruthenium metal.  $^{38}$  The N1s spectrum in Fig. 4d resolved two peaks at 399 and 398 eV ascribed to C-NH<sub>2</sub> and C-N-C, respectively.

The electrochemical performance of carbon nitride was investigated using cyclic voltammetry (CV), galvanostatic chargedischarge (GCD), and electrochemical impedance spectroscopy (EIS) tests based on a three-electrode system. Fig. 5a reveals the CV graph sample in 3M KOH solution at different scan rates  $(20 \text{ mV s}^{-1} \text{ to } 80 \text{ mV s}^{-1})$  with a broad potential window of -0.3 to 0.7 V. The decrease in specific supercapacitance as the scan rate increases is attributed to faster scan rates; electrolytes (ions) are only exchanged on the outer surface of the composite, whereas with slower scan rates, the ions are exchanged on the surface of the pore walls deeper within the composite, which results in a higher supercapacitance value. Generally, electrode materials reveal the rectangular shape of CV curves based on an electrochemical double-layer capacitor (EDLC) mechanism.<sup>39</sup> However, the electrode materials show redox peaks that follow a battery-like faradaic mechanism. The shape of CV curves also depends upon the nature of electrolytes in electrochemical properties. The deintercalation/intercalation of ions between the KOH and electrode materials and surface adsorption/desorption may

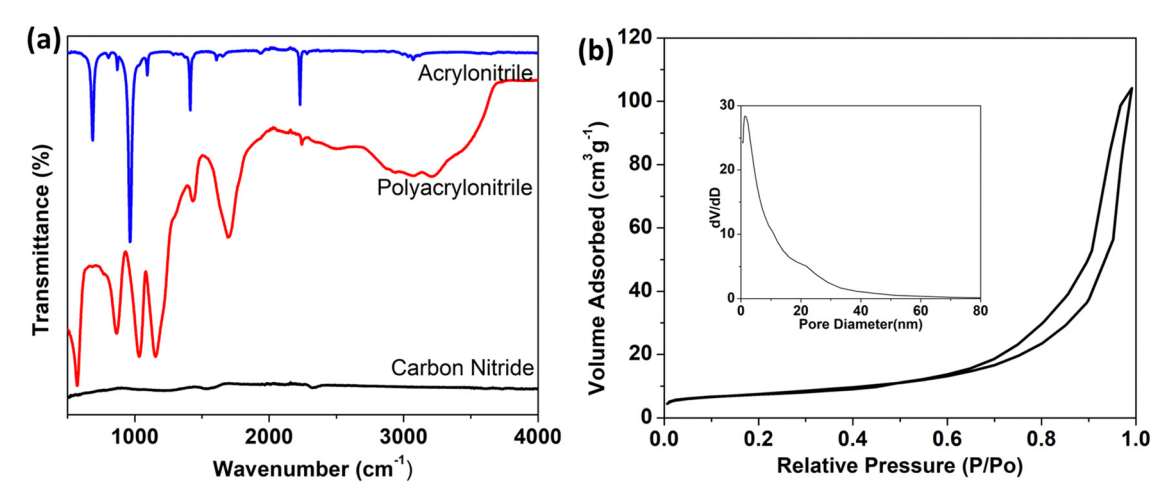


Fig. 3 (a) FTIR and (b) BET data of carbon nitride.

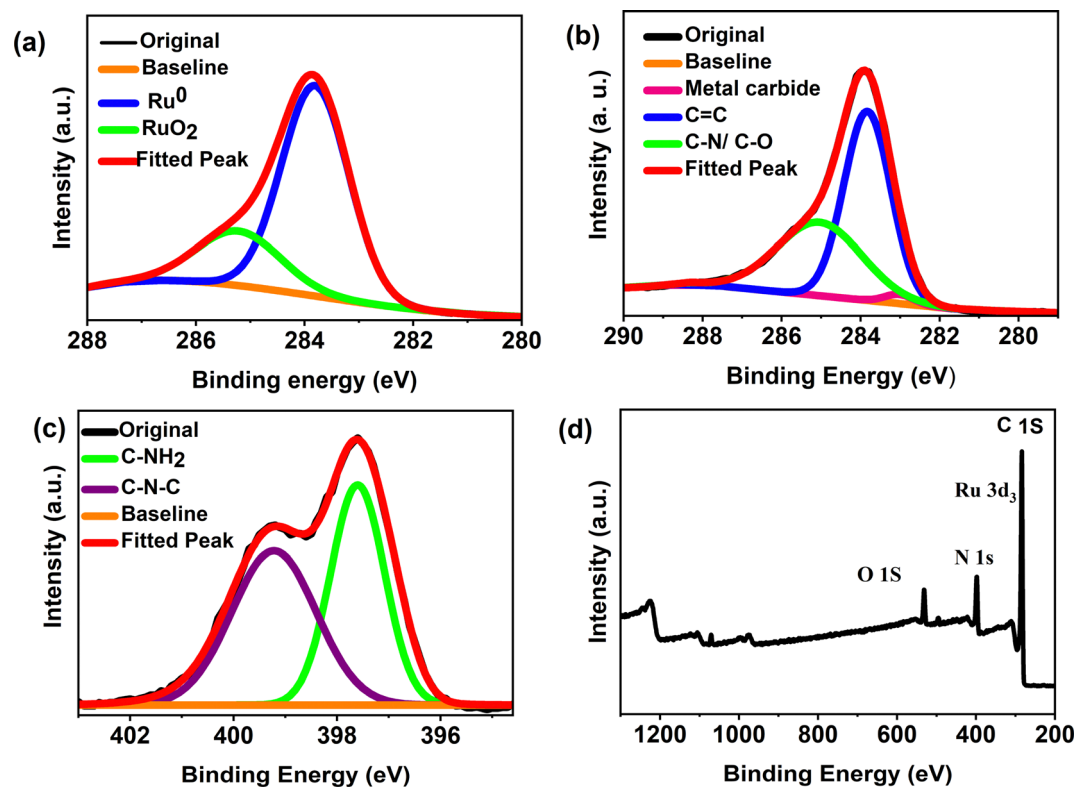


Fig. 4 XPS spectra of carbon nitride. (a) Ru 3d, (b) C 1s, (c) N 1s, and (d) survey spectra.

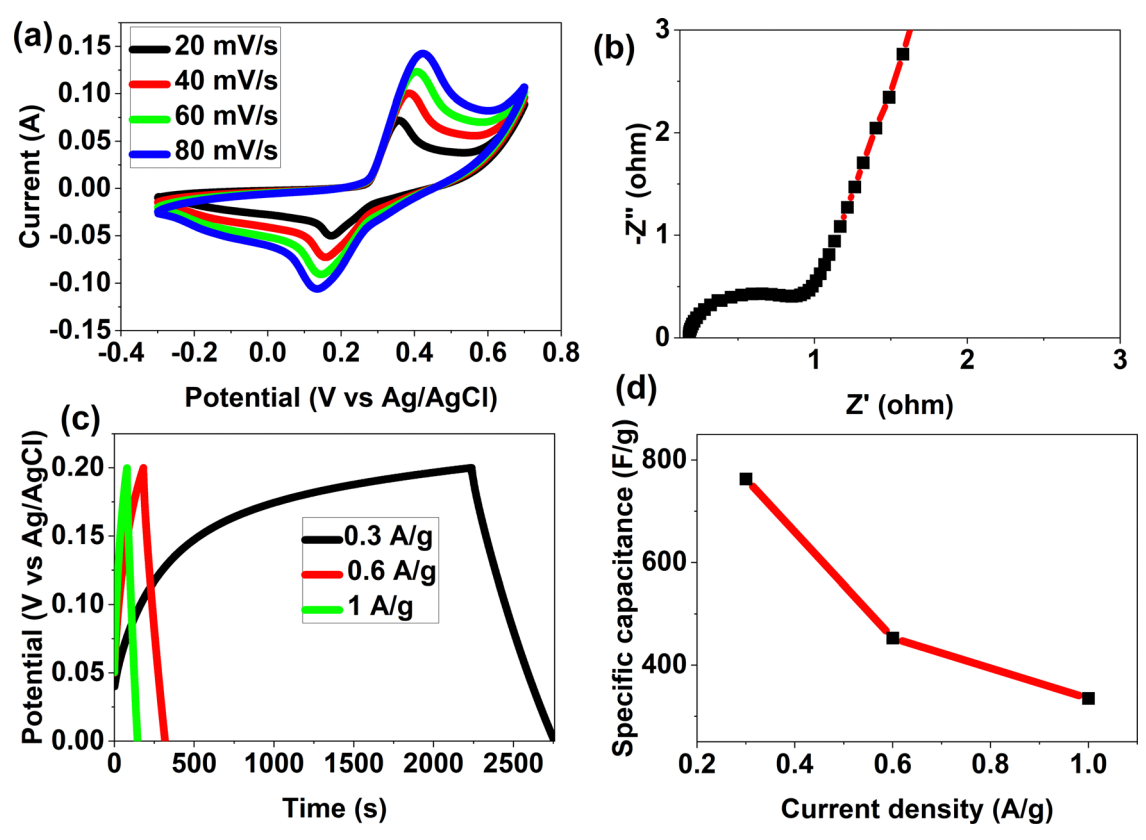


Fig. 5 Electrochemical measurements of the sample. (a) CV, (b) EIS, (c) GCD curves, and (d) specific capacitance at different current densities.

cause deviation in the rectangular CV shape. 40-43 The CV graph shows a pair of redox peaks (anodic peak: 0.13 V and cathodic peak: 0.42 V) with good rate characteristics even at a high scan rate of 80 mV s<sup>-1</sup>. Also, the redox peaks were slightly shifted along the increase in scan rate, indicating the fast redox reaction of the electrode.44 The possible redox peaks may associated with the faradaic behavior of Ru/RuO2 containing carbon nitride electrode in the presence of OH<sup>-.45,46</sup> The presence of redox peaks in the sample also suggests the pseudocapacitive material. This result indicates the assimilation of Ru/RuO2 nanoparticles in the carbon nitride structure promotes the rapid transport of ions and charge transfer that lowers the ions-diffusion process for enhancing the supercapacitor performance of the sample.<sup>47</sup> The Nyquist plot indicates a semicircle arc in the high-frequency region that shows proof of effective charge transfer behavior in the sample. 44 The rate capability of the electrode was analyzed by measuring the GCD values at different current densities (0.3, 0.6, and 1 A g<sup>-1</sup>) (Fig. 5c). The GCD curves revealed a low IR drop that provides evidence of excellent coulombic efficiency and negligible internal resistance. 48 It could be observed that specific capacitance decreased with increased current density. The possible reason may be associated with the lack of ions diffusion in the electrolyte at high current density and less utilization of the electrode surface. 49,50 The specific capacitance of the electrode was 763, 453, and 335 F g<sup>-1</sup> at 0.3, 0.6, and 1 A  $g^{-1}$  current densities, respectively (Fig. 5d). The excellent specific capacitance behavior was mainly attributed to micro/mesoporous structure, active sites for a superior redox reaction, intimate contact between Ru/RuO2 nanoparticles with amorphous carbon nitride, rapid transportation of ions, and fast electrolyte transfer process. Furthermore, our results were compared with other literature related with RuO2-based electrode materials in Table S1 (ESI†). It suggests that Ru/RuO2 nanoparticles containing amorphous carbon nitride electrodes show relatively good specific capacitance and are comparable or superior to other RuO2-based electrode materials.

#### Conclusion

This study synthesized porous carbon nitride with superior electrochemical performance using the Belousov-Zhabotinsky (B-Z) reaction as a facile, effective, and sustainable one-pot approach that gathers the activation, polymerization, and carbonization. Judicious selection of monomers with nitrogen and carbon leads to the formation of carbon nitride without a secondary source. The B-Z reaction initiates polymerization and behaves as a porogen to generate porous polymeric materials. This method is a rare design for radical polymerization since thermal initiation, photo-initiation, organic solvents, inert atmosphere, etc., are not required as an essential. Because of this simplicity, this reaction can be achieved in a standard coffee cup. The B-Z reaction is an affordable pathway and a simple technique with a potentially powerful impact on materials synthesis. This synthesis approach has a significant innovation in material science with potentially many unforeseen benefits. Finally, carbon nitride was used as electrode material for

supercapacitors. The maximum specific capacitance of 763 F g<sup>-1</sup> was obtained.

#### Author contributions

The manuscript was written through the contributions of all authors. All authors have given approval to the final version of the manuscript.

#### Conflicts of interest

There are no conflicts to declare.

## Acknowledgements

BPB would like to thank the National Science Foundation; Research Initiation Award (2000310), Joint School of Nanoscience and Nanoengineering, a member of the Southeastern Nanotechnology Infrastructure Corridor and National Nanotechnology Coordinated Infrastructure, which is supported by the National Science Foundation (Grant ECCS-1542174). TA acknowledges the Researcher Supporting Project (RSP2024R6) at King Saud University Riyadh, Saudi Arabia. The authors would like to thank Mr. Rabin Dahal for SEM imaging, Mr. Moses D. Ashie for XPS measurement and the Analytical Services Laboratory at the College of Agriculture and Environmental Sciences for their assistance with elemental analysis.

#### References

- 1 S. Ott, A. Orfanidi, H. Schmies, B. Anke, H. N. Nong, J. Hübner, U. Gernert, M. Gliech, M. Lerch and P. Strasser, Nat. Mater., 2020, 19, 77-85.
- 2 L. L. Zhang and X. S. Zhao, Chem. Soc. Rev., 2009, 38, 2520-2531.
- 3 B. P. Bastakoti, H. Oveisi, C.-C. Hu, K. C.-W. Wu, N. Suzuki, K. Takai, Y. Kamachi, M. Imura and Y. Yamauchi, Eur. J. Inorg. Chem., 2013, 1109-1112.
- 4 M. Qiao, Y. Wang, Q. Wang, G. Hu, X. Mamat, S. Zhang and S. Wang, Angew. Chem., Int. Ed., 2020, 59, 2688-2694.
- 5 H. Wang, Y. Shao, S. Mei, Y. Lu, M. Zhang, J. Sun, K. Matyjaszewski, M. Antonietti and J. Yuan, Chem. Rev., 2020, 120, 9363-9419.
- 6 S. Selvam, Y.-K. Park and J.-H. Yim, *Adv. Sci.*, 2022, **9**, 2201890.
- 7 D. Park, Y.-K. Park, S. Selvam and J.-H. Yim, J. Energy Storage, 2022, 51, 104543.
- 8 S. Selvam and J.-H. Yim, J. Energy Storage, 2023, 58, 106340.
- 9 S. Selvam and J.-H. Yim, J. Energy Storage, 2022, 45, 103791.
- 10 Y. Rangraz, M. M. Heravi and A. Elhampour, Chem. Record, 2021, 21, 1985-2073.
- 11 D. Chinnadurai, R. Rajendiran, A. R. Selvaraj, H.-J. Kim and K. Prabakar, New J. Chem., 2020, 44, 10911-10917.
- 12 M. Qiao, Y. Wang, Q. Wang, G. Hu, X. Mamat, S. Zhang and S. Wang, Angew. Chem., Int. Ed., 2020, 59, 2688-2694.
- 13 S. Y. Ejeta and T. Imae, J. Photochem. Photobiol. Chem., 2021, 404, 112955.

- 14 Y. Mai and A. Eisenberg, Chem. Soc. Rev., 2012, 41, 5969.
- 15 K. Nakashima and P. Bahadur, Adv. Colloid Interface Sci., 2006, 123-126, 75-96.
- 16 W. Luo, T. Zhao, Y. Li, J. Wei, P. Xu, X. Li, Y. Wang, W. Zhang, A. A. Elzatahry, A. Alghamdi, Y. Deng, L. Wang, W. Jiang, Y. Liu, B. Kong and D. Zhao, J. Am. Chem. Soc., 2016, 138, 12586-12595.
- 17 W.-C. Chu, B. P. Bastakoti, Y. V. Kaneti, J.-G. Li, H. R. Alamri, Z. A. Alothman, Y. Yamauchi and S.-W. Kuo, Chem. - Eur. J., 2017, 23, 13734-13741.
- 18 S. Yao, S. Xue, S. Peng, R. Guo, Z. Wu, X. Shen, T. Li and L. Wang, Appl. Phys. A: Mater. Sci. Process., 2018, 124, 758.
- 19 D. Burmeister, J. Müller, J. Plaickner, Z. Kochovski, E. J. W. List-Kratochvil and M. J. Bojdys, Chem. - Eur. J., 2022, 28, e202200705.
- 20 M. Groenewolt and M. Antonietti, Adv. Mater., 2005, 17, 1789-1792.
- 21 A. N. Zaikin and A. M. Zhabotinsky, Nature, 1970, 225, 535-537.
- 22 M. Duenas-Diez and J. Perez-Mercader, Sci. Rep., 2020, **10**, 6814.
- 23 L. Hou, M. Duenas-Diez, R. Srivastava and J. Perez-Mercader, Commun. Chem., 2019, 2, 139.
- 24 B. P. Bastakoti and J. Perez-Mercader, Angew. Chem., Int. Ed., 2017, 56, 12086-12091.
- 25 G. A. Frerichs and D. Yengi, RSC Adv., 2021, 11, 16435–16444.
- 26 R. P. Washington, W. W. West, G. P. Misra and J. A. Pojman, J. Am. Chem. Soc., 1999, 121, 7373-7380.
- 27 N. Corrigan, S. Shanmugam, J. Xu and C. Boyer, Chem. Soc. Rev., 2016, 45, 6165-6212.
- 28 M. Orbán, K. Kurin-Csörgei, A. M. Zhabotinsky and I. R. Epstein, Faraday Discuss., 2002, 120, 11-19.
- 29 L. Sciascia, F. Rossi, C. Sbriziolo, M. L. T. Liveri and R. Varsalona, Phys. Chem. Chem. Phys., 2010, 12, 11674-11682.
- 30 Y. N. Sazanov, G. N. Fedorova, G. N. Gubanova and T. E. Sukhanova, Mendeleev Commun., 2014, 24, 239-241.
- 31 V. Vijayabala, N. Senthilkumar, K. Nehru and R. Karvembu, J. Mater. Sci. Mater. Electron., 2018, 29, 323-330.

- 32 D. Z. Austin, M. A. Jenkins, D. Allman, S. Hose, D. Price, C. L. Dezelah and J. F. Conley, Chem. Mater., 2017, 29, 1107-1115.
- 33 A. Jenab, R. Roghanian, N. Ghorbani, K. Ghaedi and G. Emtiazi, Int. J. Nanomedicine, 2020, 15, 717-728.
- 34 B. P. Bastakoti, S. Guragain and J. Perez-Mercader, Chem. -Eur. J., 2018, 24, 10621.
- 35 B. P. Bastakoti and J. Perez-Mercader, Adv. Mater., 2017, 29, 1704368.
- 36 J. H. Torres, G. Franco, P. G. González, L. G. González, T. H. Quiroz, L. Z. Peredo, V. H. M. García and A. C. Rosa, J. Spectrosc., 2016, 5810592.
- 37 B. Zhang, C. Zhang, H. He, Y. Yu, L. Wang and J. Zhang, Chem. Matter., 2010, 22, 4056-4061.
- 38 J. Ji, H.-I. Joh, Y. Chung and Y. Kwon, Nanoscale, 2017, 9, 15998-16004.
- 39 S. A. Patil, I. Rabani, S. Hussain, Y.-S. Seo, J. Jung, N. K. Shrestha, H. Im and H. Kim, Nanomaterials, 2022, 12, 339.
- 40 V. Sannasi, M. Maheswari, K. Ramachandran and S. Karuppuchamy, J. Electron. Mater., 2021, 50, 6102.
- 41 Y. Wang, Y. Song and Y. Xia, Chem. Soc. Rev., 2016, 45, 5925.
- 42 P. Navalpotro, M. Anderson, R. Marcilla and J. Palma, Electro-chim. Acta, 2018, 263, 110.
- 43 M. Layegh, F. E. Ghodsi and H. Hadipour, J. Phys. Chem. Solids, 2018, 121, 375.
- 44 Y. Wang, B. Wang, R. Shi, L. Chen, Q. Che, J. Wang and P. Yang, J. Electroanal. Chem., 2022, 926, 116928.
- 45 L. Zhao, F. Di, X. Wang, S. Farid and S. Ren, Chinese J. Chem. Eng., 2023, 55, 93-100.
- 46 W. Zhang, S. Yu, H. Hu, Y. Fei, L. Chen and T. Zhang, Appl. Surf. Sci., 2023, 158285.
- 47 S. Subramani and S. Rajiv, J. Mater. Sci.: Mater. Electron., 2022, 33, 9558-9569.
- 48 S. K. Ray, B. Pant, M. Park, J. Hur and S. W. Lee, Ceram. Int., 2020, 46, 19022-19027.
- 49 Y. G. Wang, Z. D. Wang and Y. Y. Xia, Electrochim. Acta, 2005, 50, 5641-5646.
- 50 Y. Gong, D. Li, Q. Fu and C. Pan, Prog. Nat. Sci.: Mater. Int., 2015, 25, 379-385.